Monocyclopentadienyl Compounds of Manganese(II). Synthesis, Structure, Magnetism, and NMR Spectra

Frank H. Köhler,* Nikolaus Hebendanz, Gerhard Müller, and Ulf Thewalt†

Anorganisch-chemisches Institut, Technische Universität Müchen, D-8046 Garching, Federal Republic of Germany

Basil Kanellakopulos and Reinhard Klenze

Institut für Heiβe Chemie, Kernforschungszentrum Karlsruhe, D-7514 Eggenstein-Leopoldshafen, Federal Republic of Germany

Received April 22, 1986

A series of 13 manganese(II) half-sandwich compounds $[(R_ncp)MnXL]_2$, type L, and $(Rcp)MnXL_2$, type K, have been prepared on different routes. These routes include the new starting materials $Mn(DME)_2I_2$ and $[Mn_3I_6(AsEt_3)_4]_n$. In general, K is favored only when small powerful donor ligands are used. In solution K and L are in equilibrium when R = Me, X = I, and L = PMe_3. Byproducts of low solubility may force the equilibrium entirely to K, e.g., for R = H, X = I, and L = PMe_3. A systematic paramagnetic NMR study shows that the compounds may be characterized easily. In particular, the distinction between K and L, the delocalization of unpaired electrons, and hyperconjugative effects in the phosphine–transition-metal bonding are shown. According to the NMR data and to solid-state magnetic measurements all compounds have five unpaired electrons per manganese at room temperature. For $[Mecp)MnX(PEt_3)]_2$ (X = Cl (**2**), X = Br (**3**), = I (**4**)) the magnetism has been followed down to 1.25 K, and antiferromagnetic interaction with J = −4.8, −5.0, and −4.7 cm^{-1} has been found. The J values are shown to be typical for superexchange in high-spin maganese(II) dimers. As determined by X-ray crystallography **2**, **3**, and **4** are halogen-bridged centrosymmetric dimers with pseudotetrahedral metal centers. Crystals of **2** and **3** are orthorhombic, space group *Pbca*, with a = 13.691 (3)/13.869 (1) Å, b = 15.314 (2)/15.248 (1) Å, c = 14.402 (3)/14.540 (1) Å, V = 3019.6/3074.8 Å^3, and d_{calcd} = 1.265/1.435 g cm^{-3} for Z = 4. Refinement converged at R = 0.055/0.046 for 156/136 refined parameters and 1611/1572 observables. **4** is monoclinic, space group $P2_1/c$, with a = 15.099 (4) Å, b = 15.365 (3) Å, c = 14.576 (4) Å, β = 108.11 (2)°, V = 3214.1 Å^3, and d_{calcd} = 1.567 g cm^{-3} for Z = 4. Refinement converged at R = 0.071 for 227 refined parameters and 2697 observed reflections. There is a clear halogen dependence for the geometry of the central Mn_2X_2 unit. All distances and the angle X–Mn–X increase on going from Cl to I while Mn–X–Mn* decreases. The latter effect is attributed to increasing halogen repulsion.

Introduction

Transition-metal monocyclopentadienyl compounds or half-sandwiches are best known for the formal oxidation state +I of the metal. For instance, an overwhelming number of useful molecules has been obtained for the series $(CpML_x)_n$, by variation of the ligands L (CO being the most prominent) and by modifying the cyclopentadienyl. An additional dimension of reactivity can be introduced by increasing the formal oxidation state as in $(CpML_yX)_n$, where X is an anionic ligand like halide. Remarkable progress in this field has been achieved very recently by several groups.[1] However, paramagnetic manganese compounds of this type were unknown until we described $[(Mecp)MnCl(PEt_3)]_2$ and $(Mecp)MnI(PMe_3)_2$ in a preliminary report;[2] Heck et al.[3] obtained similar derivatives.

A general access to manganese(II) half-sandwiches and the knowledge of their properties are desirable for several reasons. "CpMnCl" or "(Mecp)MnCl" has been mentioned as an intermediate,[4] and patents claim the use of $(R_ncp)MnX$ in the synthesis of corresponding $(R_ncp)Mn(CO)_3$,[5] useful as antiknock additives. It is unknown, however, as to whether Grignard analogues or half-sandwiches were involved.

Stabilization of radicals by $CpMnL_2$ fragments could lead to similar 17-electron manganese complexes.[6] From the hyperfine coupling constants it appears that, e.g., $\{[CpMn(CO)_2]_2(\mu\text{-pyrazine}]^{\bullet-}$, described by Kaim,[6b] contains a ligand radical. By contrast, the oxidation products of $CpMn(CO)_2L$ reported by Sellmann's[6a] and Huttner's[6c] groups are metal-centered radicals. These differ in turn from the half-sandwiches reported here by their spin state.

Finally, the 17-electron complex $[(Mecp)Mn(CO)_2L]^+$ (L = 3- or 4-substituted pyridine) has been shown by Kochi[7] to be a very short-lived intermediate in the ligand substitution reaction of cymantrene derivatives. In this reaction steric and electronic effects are nicely understood for specific ligands. Nevertheless, the spin state of the important intermediate is unknown. We report here on new manganese(II) half-sandwiches with emphasis on their magnetic, structural, and NMR properties.

† Visiting professor from the University of Ulm (1983/1984).

(1) (a) Kölle, U.; Fuss, B.; Kouzami, F.; Gersdorf, J. *J. Organomet. Chem.* **1985**, *290*, 77 (cit. lit.) (b) Bunel, E. E.; Valle, L.; Manriquez, J. M. *Organometallics* **1985**, *4*, 1680. (c) Wright, M. E.; Nelson, G. O.; Glass, R. S. *Organometallics* **1985**, *4*, 245. (d) Tilley, T. D.; Grubbs, R. H.; Bercaw, J. E. *Organometallics* **1984**, *3*, 279. (e) Albers, M. O.; Oosthuizen, H. E.; Robinson, D. J.; Shaver, A.; Singleton, E. *J. Organomet. Chem.* **1985**, *282*, C29. (f) Lehmkuhl, H.; Mehler, G. *Chem. Ber.* **1985**, *118*, 2407.

(2) (a) Ackermann, K.; Cao, R.; Hebendanz, N.; Köhler, F. H.; Thewalt, U. In *Chemiedozententagung 1984*; Verlag Chemie: Weinheim, 1984; p 95. (b) Köhler, F. H.; Hebendanz, N.; Thewalt, U.; Kanellakopulos, B.; Klenze, R. *Angew. Chem.* **1984**, *96*, 697; *Angew. Chem., Int. Ed. Engl.* **1984**, *23*, 721.

(3) Heck, J.; Massa, W.; Weinig, P. *Angew. Chem.* **1984**, *96*, 699; *Angew. Chem., Int. Ed. Engl.* **1984**, *23*, 723.

(4) (a) Coffield, T. H.; Sandel, V.; Closson, R. D. *J. Am. Chem. Soc.* **1957**, *79*, 5826. (b) Fischer, E. O.; Breitschaft, S. *Chem. Ber.* **1966**, *99*, 2213.

(5) Shapiro, H. U.S. Patent 2916504 and 2916505, 1959.

(6) (a) Sellmann, D.; Müller, J.; Hofmann, P. *Angew. Chem.* **1982**, *94*, 708; *Angew. Chem., Int. Ed. Engl.* **1982**, *21*, 691. (b) Kaim, W.; Gross, R. *Angew. Chem.* **1984**, *96*, 610; *Angew. Chem., Int. Ed. Engl.* **1984**, *23*, 614. (c) Winter, A.; Huttner, G.; Zsolnai, L.; Kroneck, P.; Gottlieb, M. *Angew. Chem.* **1984**, *96*, 986; *Angew. Chem., Int. Ed. Engl.* **1984**, *23*, 975. (d) Sellmann, D.; Müller, J. *J. Organomet. Chem.* **1985**, *281*, 249. (e) Winter, A.; Huttner, G.; Jibril, J. *J. Organomet. Chem.* **1985**, *286*, 317.

(7) Zizelman, P. M.; Amatore, C.; Kochi, J. K. *J. Am. Chem. Soc.* **1984**, *106*, 3771.

0276-7333/87/2306-0115$01.50/0

Scheme I

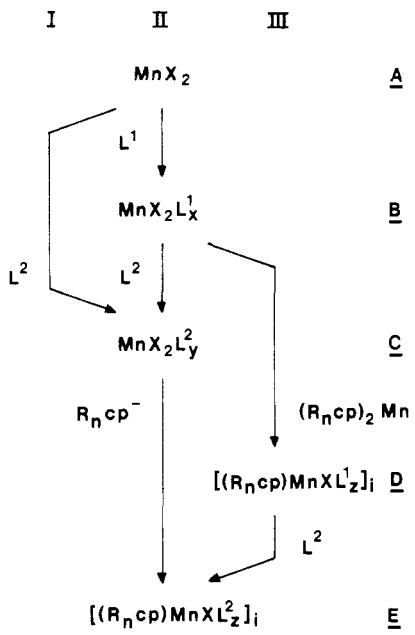

Results

Formation and Properties of Compounds. When 1,1-dimethylmanganocene is prepared by reaction of the colorless THF adduct of $MnCl_2$ and methyl cyclopentadienide, a light green color can be observed after addition of about half of the Cp reagent. This is probably the most simple reaction among a number of routes depicted in Scheme I; it is generalized as route I: the starting halide A is first converted to a solvate or adduct C and then directly to the half-sandwich complex E. The compounds $[(Mecp)MnCl(THF)]_2$ (**1**). $[(Mecp)MnI(AsEt_3)]_2$ (**7**), $[CpMnI(PMe_3)]_2$ (**9**), $(Mecp)MnCl(PMe_3)_2$ (**11**), and (Mecp)MnI(dmpe) (**13**) [dmpe = 1,2-bis(dimethylphosphino)ethane] are obtained in this way. The actual stoichiometry and structure of these half-sandwiches will be discussed later. The intermediates C may be poorly soluble so that the yield of E is low. In such a case it is advantageous to choose route II and to prepare an intermediate adduct, B. Intermediates B and C may be isolated; examples are MnI_2(1,2-dimethoxyethane)$_2$, $MnI_2(PEt_3)_2$[8] or the triethylarsine derivative of MnI_2 which analyzed for $[Mn_3I_6(AsEt_3)_4]_n$. The structure of the latter adduct is unknown; the presence of six- and four-coordinate manganese may be expected, however. Route II can as well be realized in a one-pot synthesis. The compounds $[(Mecp)MnBr(PEt_3)]_2$ (**3**), $[(1,2\text{-}Me_2cp)MnI(PEt_3)]_2$ (**6**), and $[CpMnI(PEt_3)]_2$ (**8**) are obtained on route II.

The comproportionation of an intermediate like B with manganocenes shown in route III is another possibility. It is efficient when the manganocene is highly soluble. For example, Cp_2Mn does not react and routes I and II have to be used to introduce the parent ligand Cp. Manganese(II) half-sandwiches are susceptible to an exchange of the ligand L depending on the relative binding ability of L. Therefore they may act as an intermediate, D, in route III giving $[(Mecp)MnCl(PEt_3)]_2$ (**2**), $[(Mecp)MnI(PEt_3)]_2$ (**4**), $[(Me_3Sicp)MnI(PEt_3)]_2$ (**5**), and $(Mecp)MnI(PMe_3)_2$ (**12**).

The yields depend on the solubility of the product and the preparation method; 80% may be exceeded after optimization. Manganese(II) half-sandwiches are light to dark green in solution and in the solid state. The green color points to a bonding situation unlike in Grignard analogues RMnX which are beige to brownish.[9] As an exception, **13** becomes red-brown on cooling, a phenomenon which is under study. All compounds are very sensitive to oxygen and moisture, they are quite stable thermally, and the solubility of the phosphine derivatives decreases on going from toluene or benzene to pentane and from THF to dioxane and diethyl ether. Replacing chloride by bromide and iodide increases the solubility in diethyl ether. The THF and $AsEt_3$ adducts **1** and **7** are much more labile and decompose in most solvents except diethyl ether. In THF **7** is transformed to **1**. Elemental analyses and the mass spectrum of **13** show **11**–**13** to contain two additional donor molecules while **1**–**9** contain only one, thus giving rise to a dimeric structure. Cryoscopy confirms the dimeric structure of **4** in benzene; the experimental value of 790 daltons (calcd 758) is well within the 5% error limit. On the other hand, for **12** a mean value of 354 daltons (calcd 413/674 for the monomer/dimer) from successive measurements with 370, 350, and 342 daltons in benzene suggests an equilibrium

$$2(Mecp)MnI(PMe_3)_2 \rightleftharpoons [(Mecp)MnI(PMe_3)]_2 + 2PMe_3$$
10

with one-third of the original monomers having dimerized.

So far we are unable to isolate a manganese(II) half-sandwich having four or five alkyls per cyclopentadienyl by the methods described above. Thus, the attempted synthesis of $[(Me_4cp)MnI(PEt_3)]_2$ by adding PEt_3 to a mixture of MnI_2 and $(Me_4cp)_2Mn$ gives $MnI_2(PEt_3)_2$,[8] the most simple type of a manganese dihalide phosphine adduct known so far; the manganocene is recovered and identified by NMR.[10] Similarly, the reaction of equimolar amounts of $(Etme_4cp)Li$ and $MnCl_2(THF)_x$ yields $(Etme_4cp)_2Mn$ and leaves half of the halide unreacted.

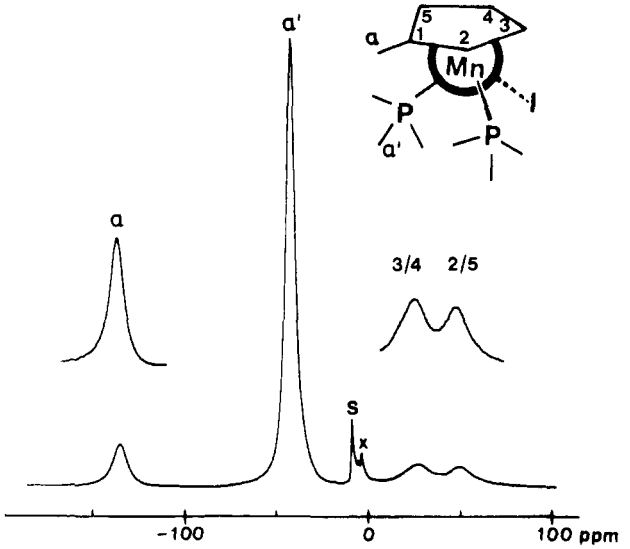

Figure 1. ^1H NMR spectrum of $(Mecp)MnI(PMe_3)_2$ (**12**) in C_6D_6 at 305 K (S = solvent; X = PMe_3). The shift scale is linked arbitrarily to Me_4Si as zero since experimental spectra do not give uniform paramagnetic shifts.

Paramagnetic NMR Spectra. Manganese(II) half-sandwiches yield typical ^1H NMR spectra; examples are given in Figures 1 and 2. The assignment follows from the signal areas and from chemical modification. If, for instance, we replace Mecp (Figure 1) by Cp (Figure 2), the

(8) Hebendanz, N.; Köhler, F. H.; Müller, G. *Inorg. Chem.* **1984**, *23*, 3043.

(9) Friour, G.; Cahiez, G.; Normant, J. F. *Synthesis* **1984**, 37.

(10) Hebendanz, N.; Köhler, F. H.; Müller, G.; Riede, J. *J. Am. Chem.* **1986**, *108*, 3281.

Table I. Paramagnetic ^1H and ^{13}C Shifts at 298 K (δ_{298}^{para}) of Manganese(II) Half-Sandwiches

		cyclopentadienyl			phosphine		
compd	nucleus	2/5	3/4	α	α′	β′	other
[(Mecp)MnCl(PEt$_3$)]$_2$ (**2**)	$^1H^a$	62.9	16	−145	−28.4	−5.7	
[(Mecp)MnBr(PEt$_3$)]$_2$ (**3**)	^1H	56.9	*c*	−140	−26.8	−4.3	
[(Mecp)MnI(PEt$_3$)]$_2$ (**4**)	$^1H^a$	55.0	21	−135	−23.9	−7.5	
	^{13}C	*b*	*b*	266	−374	−117	C1^b
[(Me$_3$Sicp)MnI(PEt$_3$)]$_2$ (**5**)	^1H	−51	38.7		−22.3	−5.4	SiCH$_3$ −10.9
[(1,2-Me$_2$cp)MnI(PEt$_3$)]$_2$ (**6**)	^1H	39^d		−158	−23.7	−4.2	H1 22^d
[(Mecp)MnI(AsEt$_3$)]$_2$ (**7**)	^1H	52.3	16	−137	−1.6	−9.3	
[CpMnI(PEt$_3$)]$_2$ (**8**)	$^1H^a$	47.5			−22.8	−6.7	
	^{13}C	*b*			−234	−73.1	
[CpMnI(PMe$_3$)]$_2$ (**9**)	^1H	43.5			−19.9		
CpMnI(PMe$_3$)$_2$ (**10**)	^1H	43.5			−35.0		
(Mecp)MnCl(PMe$_3$)$_2$ (**11**)	^1H	54.2	23	−151	−38.7		
(Mecp)MnI(PMe$_3$)$_2$ (**12**)	$^1H^a$	63.5	38.5	−146	−45.8		
	^{13}C	*b*	*b*	294	−554		C1^b
(Mecp)MnI(dmpe) (**13**)	^1H	52.9	30.3	−161	CH_3− 54.7		
					CH_2− 31.4		
	^{13}C	*b*	*b*	309	CH_3− 693		
					CH_2− 98.7		C1^b

^{a} From a variable temperature study. ^{b} Not observed for S/N reason. ^{c} Hidden under the solvent. ^{d} Symmetry-adapted numbering with C1 lying on the C_2 axis of the isolated ligand.

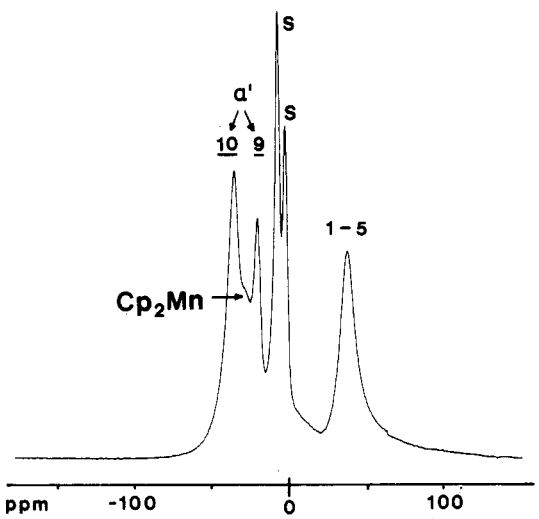

Figure 2. ^1H NMR spectrum of [CpMnI(PMe$_3$)]$_2$ (**9**) yielding some CpMnI(PMe$_3$)$_2$ (**10**) after dissolution in toluene-d_8 at 305 K (see text for details) (S = solvent).

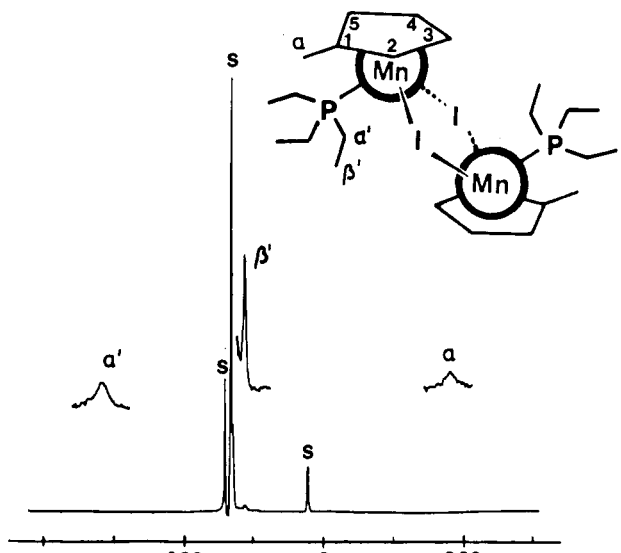

Figure 3. ^{13}C NMR spectrum of [(Mecp)MnI(PEt$_3$)]$_2$ (**4**) in toluene-d_8 at 360 K (S = solvent).

splitting of the cyclopentadienyl signal (H2/5 and H3/4) and the Hα signal disappear. The similarity to the NMR spectra of manganocenes is also helpful, and the arguments for distinguishing H2/5 and H3/4 can be taken from our recent work.[10] The signal widths, Δ^{exptl}, depend on the temperature and, unexpectedly, on the halogen. The effect is most obvious for Hα of **2**, **3**, and **4** where Δ^{exptl} drops from 7.0 to 3.5 and 2.7 kHz at 381 K. Optimum conditions are thus met for iodo derivatives at high temperature.

In the ^{13}C NMR we observe the phosphine carbons and Cα as shown in Figure 3. The signals for C1–5 are expected to be rather broad, and our signal-to-noise ratio (cf. Figure 3) is insufficient to detect these carbons even after optimizing as just mentioned. It can, however, be estimated from the Cα signal shifts, and the complete ^{13}C spectra of the analogous ether adducts of (Mecp)$_2$Mn[10] that C1–5 should appear between 1000 and 1600 ppm to high frequency at 298 K. A collection of the NMR data is given in Table I. Attempts to record the ^1H spectrum of **1** in C_6D_6, toluene-d_8, $CDCl_3$, or CD_2Cl_2 fail due to decomposition. Even in dioxane-d_8 we merely observe (Mecp)$_2$Mn.

The phosphine proton signals Hα are especially useful because they allow the distinction between mono- and dinuclear complexes. Comparison of **2**–**4** with **11** and **12**

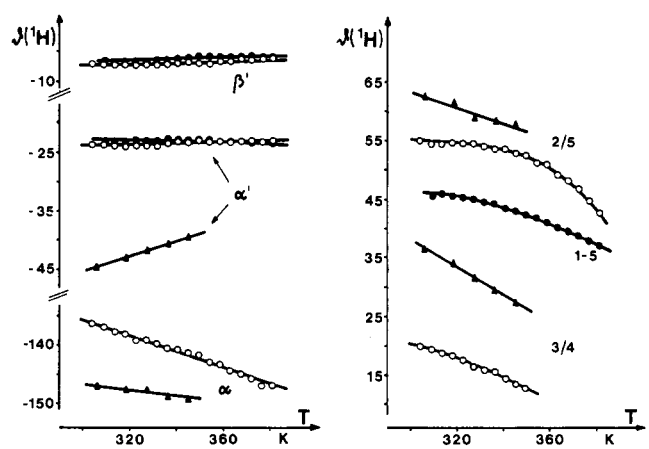

Figure 4. Temperature behavior of the ^1H signals of [(Mecp)-MnI(PEt$_3$)]$_2$ (**4**; ○), [CpMnI(PEt$_3$)]$_2$ (**8**; ●) and (Mecp)MnI(PMe$_3$)$_2$ (**12**; ▲).

in Table I shows that Hα′ of the dimers appears some 15 ppm to lower frequency than in the case of **11** and **12**. One puzzling fact is that analytically pure samples of **11** and **12** always show a signal for free PMe$_3$ (cf. Figure 1). This

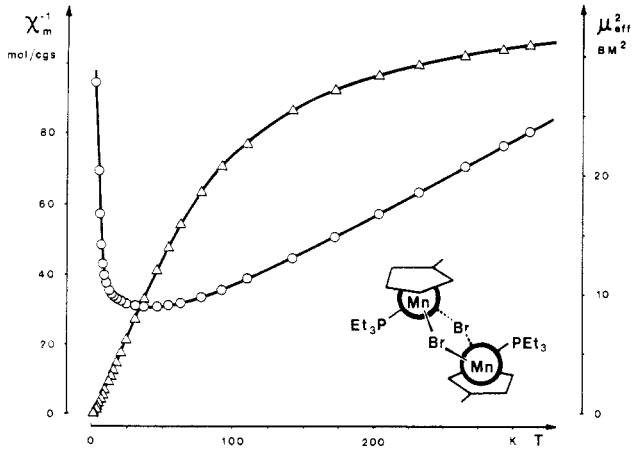

Figure 5. Temperature dependence of χ_m^{-1} and μ_{eff}^2 for $[(Mecp)MnBr(PEt_3)]_2$ (**3**).

is clearified by temperature-dependent studies. In Figure 4 the reduced paramagnetic shifts $\vartheta(^1H) = \delta^{para}T/298$ vs the temperature are depicted.

Since $\vartheta(^1H)$ is proportional to the hyperfine coupling, it should be constant in simple cases. This is actually found for the phosphine protons Hα' and Hβ' of the dimers **4** and **8**. By contrast ϑ(Hα') of **12** is temperature dependent and moves toward ϑ(Hα') of **4** and **8** with increasing temperature. We conclude that in toluene the monomer **12** is in equilibrium with the dimer **12a** and PMe_3. The interconversion of **12** and **12a** is fast on the NMR time scale, yielding an averaged signal for Hα'. The slope of the $\vartheta(^1H\alpha')$ curve says that the dimer **12a** is favored with increasing temperature. The equilibrium is proven independently by the cryoscopic measurement given above.

A different behavior is found when $[CpMnI(PMe_3)]_2$ (**9**) is dissolved in toluene. As can be seen in Figure 2 there is a signal Hα' for a mononuclear species at higher frequency from the expected one of the dimer **9**. After the sample is heated to 390 K, the signal of the dinuclear compound disappears irreversibly at the expense of that of the mononuclear compound and a cream colored precipitate is formed. These NMR findings show the following reaction to take place.

$$2[CpMnI(PMe_3)]_2 \rightarrow 2CpMnI(PMe_3)_2 + Cp_2Mn + MnI_2$$

Actually, we observe the additional ^1H signal of manganocene. In agreement with its unusual temperature behavior[10] the Cp_2Mn signal is hidden completely under Hα' of the monomer **10** at higher temperature. We note that the Cp signal shifts for **9** and **10** are too similar to be resolved. This is also reflected in the line width which is much larger in Figure 2 than for the corresponding Cp signal of **8**. The precipitate mentioned above clearly is MnI_2 together with some Cp_2Mn.

Another aim of the temperature-dependent NMR studies is to detect the electron exchange in the half-sandwich dimers similar to our work on $[CpCrCl_2]_2$.[11] Indeed, Figure 4 reveals a variation of $\vartheta(^1H)$ with temperature, but the effect is very small and not uniform. We therefore prefer information from the magnetic susceptibility of powdered samples.

Solid-State Magnetic Measurements. Between 333 and 1.25 K the series $[(Mecp)MnX(PEt_3)]_2$ with X = Cl (**2**), Br (**3**), and I (**4**) has a magnetic behavior typical for

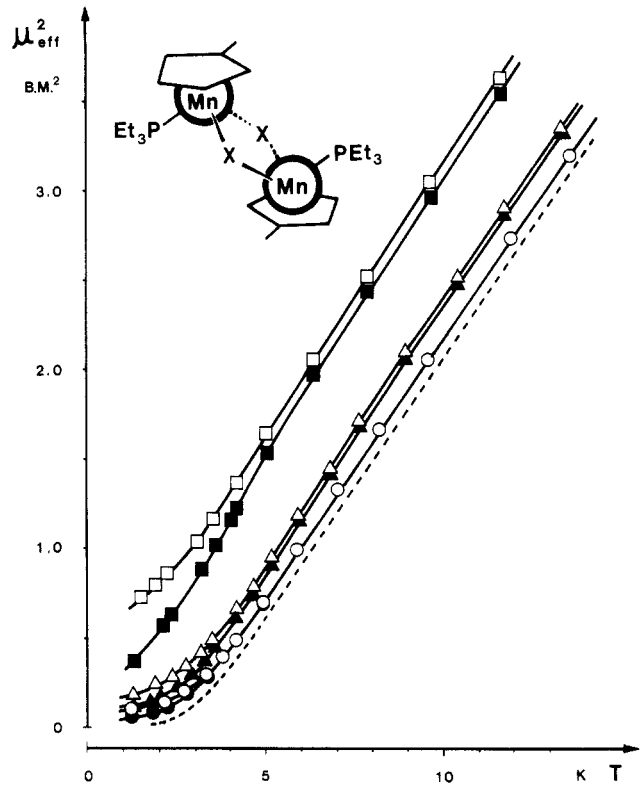

Figure 6. Field and temperature dependence of μ_{eff}^2 for samples of $[(Mecp)MnX(PEt_3)]_2$ X = Cl (△/▲), Br (○/●), and I (□/■); open signs, 0.3 T; full signs, 1.5 T. Broken line: calculated for $g = 2$ and $J = -5$ cm^{-1}.

antiferromagnetic coupling in binuclear high-spin Mn(II) complexes (data cf. supplementary material). This is shown for **3** in Figure 5 by the inverse molar susceptibility, χ_m^{-1}, and the square of the effective magnetic moment, $\mu_{eff}^2 = (3k/N\beta^2)\chi_m T$. Compounds **2** and **4** give almost identical results. χ_m^{-1} passes through a minimum near 40 K, raises sharply below 10 K, and joins a Curie–Weiss straight line above 150 K. From the slope above 230 K μ_{eff} = 6.0, 6.06, and 6.08 μ_B are obtained for **2**, **3**, and **4** which is slightly above the spin-only value expected for five unpaired electrons.

The exchange coupling in binuclear complexes is given by[12]

$$\chi_m = \tfrac{1}{2}\frac{Ng^2\beta^2}{3kT}\frac{\sum S(S+1)(2S+1)\exp[-JS(S+1)/kT]}{\sum(2S+1)\exp[-JS(S+1)/kT]}$$

where g is the electron g factor, J is the exchange coupling constant, the other symbols have the usual meaning, and in our case the sums include the five possible values of the total spin S. Fits of the experimental data to the above equation yield $g = 2.02$ and $J = -4.8$ cm^{-1} for **2**, $g = 2.02$ and $J = -5.0$ cm^{-1} for **3**, and $g = 2.00$ and $J = -4.7$ cm^{-1} for **4** where all g are ±0.02 and all J ±0.1 cm^{-1}. Within the error limits g corresponds to the theoretical value for a $^6A_1$ complex, and the calculated curves follow the experimental data remarkably well except for small deviations below 5 K. Addition of a biquadratic exchange term[12] does not improve the fit. The magnetism can therefore be understood without the influence of high order exchange interactions. Measurements at seven different field strengths (from 0.3 to 1.5 T) reveal some field dependence between 1.3 and 16 K (supplementary material). The

(11) Köhler, F. H.; Cao, R.; Ackermann, K.; Sedlmair, J. *Z. Naturforsch., B: Anorg. Chem., Org. Chem.* **1983**, *38B*, 1406.

(12) Hatfield, W. E. In *Theory and Applications of Molecular Paramagnetism*; Boudreaux, E. A., Mulay, L. N., Eds.; Wiley: New York, 1976; p 349. The equation is adapted to our χ_m values per manganese.

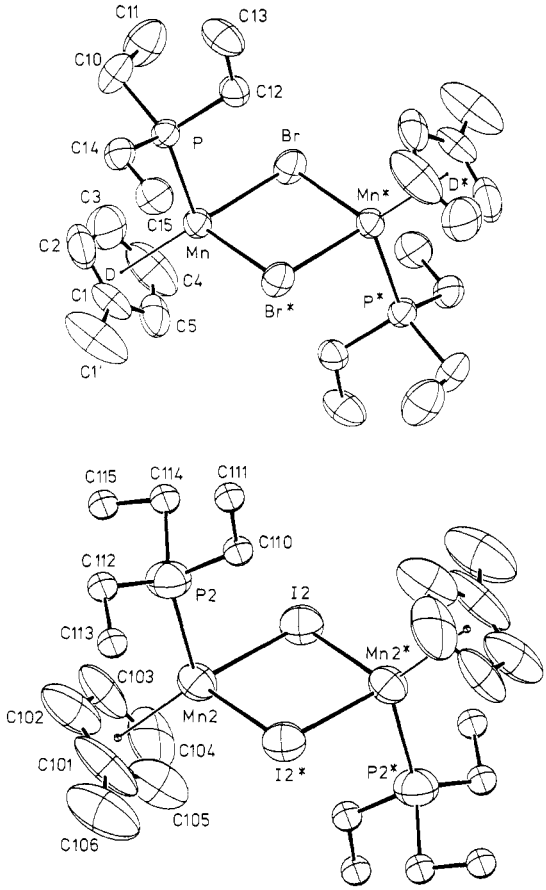

Figure 7. Molecular structures of **3** and **4** (ORTEP, thermal ellipsoids 50%, isotropically refined atoms in **4** with arbitrary radii, hydrogen atoms omitted). The structure of **2** is virtually identical with that of **3**.

extreme values are shown in Figure 6 together with the theoretical curve for $g = 2$ and $J = -5$ cm^{-1}. All curves are parallel to the theoretical one. We therefore attribute the deviations to paramagnetic impurities, most probably to Mn^{2+}. In this case the impurities amount to 0.9, 0.3, and 3.1% for **2**, **3**, and **4**, respectively. The field dependence below 15 K (observable for **3** below 5 K only) is 8, 3, and 11% for **2**, **3**, and **4**; it may be explained by magnetic saturation of the impurities.

Molecular Structure of 2, 3, and 4. In an attempt to relate the exchange coupling constants to structural parameters, the molecular structures of **2**, **3**, and **4** were determined by X-ray crystallography. All three compounds are centrosymmetric dimers with halogen bridges between the manganese centers (Figure 7). The Mn–X–Mn bridges are symmetrical (Table II). The metal centers are pseudotetrahedrally coordinated by the cyclopentadienyl rings, the P atoms of the phosphine donors, and the two bridging halogens. Actually, **2** and **3** are isostructural with corresponding close resemblances in the overall molecular structures and even in the thermal behavior of most atoms. **4** occurs in two crystallographically independent dimers, but again, crystallographic inversion symmetry is imposed on the molecules. As a consequence, the differences between the structural parameters of **2** and **3** are rather small. Only the iodo bridges in **4** cause a major lengthening of the key distances of the Mn_2X_2 four-membered ring (Tables II and III). As is evident from Table II, the increasingly longer Mn–X distances upon going from X = Cl to X = I are accompanied by a slight, but significant decrease in the Mn–X–Mn* angles, while X–Mn–X* increases only very little. The distances Mn···Mn*

Table II. Important Interatomic Distances (Å) and Angles (deg) for $[(Mecp)MnX(PEt_3)]_2$ (X = Cl (2), Br (3), and I (4))[a]

	2	3	4[b]
		Bond Distances	
Mn–X	2.483 (2)	2.634 (1)	2.866 (4)/2.872 (3)
Mn–X*	2.480 (2)	2.627 (1)	2.864 (4)/2.859 (4)
Mn–P	2.567 (2)	2.560 (2)	2.581 (7)/2.571 (7)
Mn–D[c]	2.17	2.16	2.16/2.18
Mn–C1	2.522 (8)	2.476 (8)	2.54 (3)/2.53 (2)
Mn–C2	2.580 (9)	2.542 (9)	2.55 (3)/2.63 (4)
Mn–C3	2.50 (1)	2.47 (1)	2.53 (3)/2.48 (3)
Mn–C4	2.418 (9)	2.362 (9)	2.41 (3)/2.40 (4)
Mn–C5	2.404 (8)	2.401 (8)	2.39 (3)/2.42 (3)
		Bond Angles	
X–Mn–X*	89.8 (2)	91.5 (1)	92.8 (2)/94.2 (2)
X–Mn–P	98.9 (1)	98.1 (1)	97.5 (2)/96.5 (2)
X*–Mn–P	99.3 (2)	98.6 (1)	96.1 (2)/98.4 (2)
X–Mn–D	124.1	124.5	124.7/122.3
X*–Mn–D	123.2	122.2	123.3/120.4
D–Mn–P	115.7	116.1	115.9/119.3
Mn–X–Mn*	90.2 (2)	88.5 (1)	87.2 (1)/85.8 (1)

[a] Numbering scheme see Figure 7; atoms with and without an asterisk are related by a center of symmetry; esd's in units of the last significant figure in parentheses. [b] Both values for the two crystallographically independent molecules are given. [c] D = center of the five-membered ring.

Scheme II

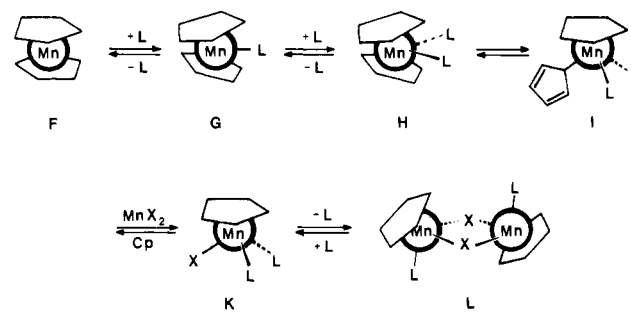

across the four-membered ring are too long to be considered bonding and increase from **2** to **4** as expected (Table III). The geometrical details of the Mn_2X_2 ring are considered further in connection with the magnetic data below.

Both, the Mn–P as well as the Mn–C distances in **2**, **3**, and **4** are directly indicative of the high-spin d^5 state of the Mn(II) center. They are noticeably longer than comparable bonds to low-spin Mn(II) but agree reasonably well with those in other high-spin complexes, as, e.g., $(Et_3P)_2MnI_2$,[8] $(Me_3Sicp)_2Mn$,[10] or $Cp_2Mn(TMEDA)$.[3]

Discussion

It appears from the results that the possibility to isolate manganese(II) half-sandwiches is a consequence of the low stability of manganocenes. One η^5-Cp is removed easily by donor molecules and excess of halide, while the second Cp resists further replacement under the conditions employed. The title compounds are hence species of preferred stability halfway between manganocenes and solvated manganese(II) halides so that both may serve as starting materials. Depending on the nature of the auxiliary ligands L, further intermediates shown in Scheme II must be taken into account. When no halide is present, G and H may be isolated as has been shown by Weed, Rettig, and Wing[13] for L = 3,5-dichloropyridine and by Wilkinson's group[14]

(13) Weed, J. F.; Rettig, M. F.; Wing, R. M. *J. Am. Chem. Soc.* **1983**, *105*, 6510.

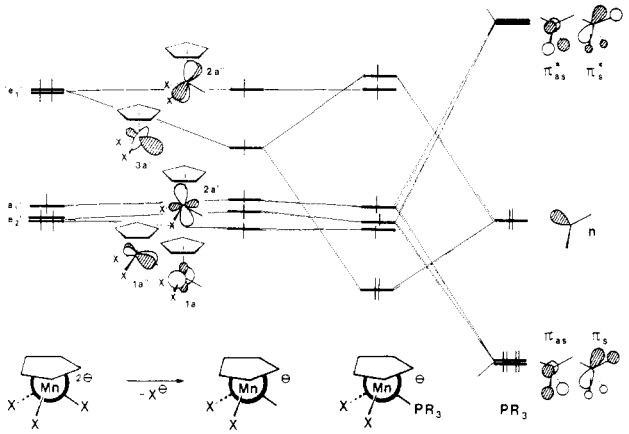

Figure 8. Qualitative MO diagram for the interaction of a $[CpMnX_2]^-$ fragment and a phosphine.

for L = PR_3 and L_2 = dmpe. The interconversion of H and I is plausible from Heck's work[3] which shows that I may be isolated with L_2 = TMEDA.

As to whether the monomeric (K) or dimeric (L) half-sandwich is more stable depends on various factors. Our series shows that the stability of the monomeric complexes is increased if the ligand L has one or more of the following properties: low steric demand, high donor power, and chelating ability. The energy difference between K and L is small enough so that the variation of the cyclopentadienyl or a change from solution to the solid state selects the monomeric or the dimeric species. Thus, we find type K only with the sterically favorable PMe_3 or the chelating dmpe. However, PMe_3 may be insufficient to stabilize K because changing Mecp in the monomers **11** and **12** for Cp gives a solid material, **9**, with dimeric units L even after crystallization in the presence of excess PMe_3. Redissolution of **9** gives the monomer **10** in a reaction which is most probably driven by the low solubility of the byproducts MnI_2 and notably Cp_2Mn.

The failure to prepare derivatives with highly alkylated cyclopentadienyls is related to the reactivity differences of low- and high-spin manganocenes and their equilibrium concentration.[10] High-spin manganocene has a metal–ligand distance which is about 0.3 Å longer than in low-spin isomers,[15] and therefore the latter should have a much higher activation energy for the displacement of a cyclopentadienyl. Clearly, at the end of all routes described above, polyalkylmanganocenes will be obtained instead of the polyalkylated half-sandwiches as long as the latter are high spin. As found earlier the high-spin/low-spin isomer ratio at a given temperature decreases rapidly as the number of alkyls per Cp is increased.[10]

Information from Paramagnetic NMR. As for many other paramagnetic Cp derivatives, NMR spectroscopy is a very useful tool for the structural characterization of manganese(II) half-sandwiches in solution. Here we draw attention to the fact that in the phosphine ligands the signals of Hα' and Cα' are much more shifted than the β' resonances. Also, very different $\delta^{para}(C\alpha')$ are found for **13**. This means that electron spin density is transferred selectively to nuclei which are separated from the metal by two bonds. The origin is the π,σ-interaction illustrated

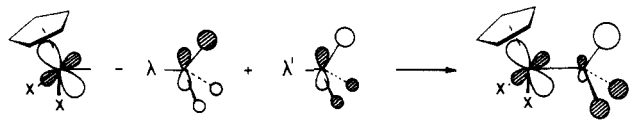

Figure 9. Selective spin transfer from **2a'** to nuclei next to phosphorus in phosphines.

in Figure 8. For simplicity we examine the 17-electron species $[CpMnX_2(PR_3)]^-$ rather than dimers like **1–9**. It results after $[CpMn(PR_3)]^+$ is removed from the dimer and has the additional advantage of being easily comparable to $CpMnX(PR_3)_2$ which stands for **10–13**. To obtain the energy level ordering of the frontier orbitals, we start with $[CpMX_3]^{2-}$. Its orbital scheme is, of course, very similar to the well-known examples $CpML_3$ and Cp_2M;[16] a treatment neglecting the π-acceptor levels of Cp^- has been given for $CpTiCl_3$.[17] We expect $[CpMnX_3]^-$ to be high spin because the three halides are less efficient donors with a smaller level splitting than Cp^- in Cp_2Mn which exists in a low-spin/high-spin equilibrium. Similar to $CpM(CO)_2$(ligand) complexes[18] we remove one halide and obtain the frontier orbitals for $[CpMnX_2]^-$. This in turn is allowed to interact with a phosphine. Filling in the five electrons gives the high-spin species (as found experimentally) because the donor ability of two halides and one phosphine—although leading to a larger overall level splitting than in $[CpMnX_3]^{2-}$—is still worse than that of Cp^-.

The phosphine ligand obtains spin density from the electron in 3a' mediated by the σ-bonds. In addition the phosphine P–C bonds, taken as π- and π^*-sets in Figure 8, can interact with 1a'' and 2a'. One of the two orbital interactions is visualized in Figure 9. The result is an extra spin density at Cα' as manifested in the large ^{13}C signal shifts. Correlation effects accompanying σ-delocalization may also cause large differences in the signal shifts of α- and β-carbon atoms. Since, however, the $\delta^{para}(C\alpha')$ of **13** depend strongly on the dihedral angle (vide infra), hyperconjugation should dominate.

These findings provide direct experimental evidence for the π-interaction of a transition metal and the P–R bonds of a phosphine ligand. π-Interactions of phosphines in general have been discussed controversly in complex chemistry for a long time. Recent calculations[19] show that back-bonding from a transition metal to PH_3 occurs into P–H π^*-orbitals and that phosphorus d orbitals are unnecessary to account for back-bonding.

From Figures 8 and 9 it is clear that paramagnetic NMR should be a general method to detect back-bonding in EX_3 complexes. X must contain an observable nucleus separated from a suitable paramagnetic metal center by two and three bonds so that both signal shifts can be compared. Another complex where we have found hyperconjugation to phosphine is $MnI_2(PEt_3)_2$.[8]

Another consequence of hyperconjugation is the striking shift difference for the dmpe signals in **13** (cf. Table I). As can be seen from Figure 10 only one signal appears for Hα''. We thus have a fast ligand permutation or a fast conformational change of the MnP_2C_2 ring. In the equilibrium conformation the two P–Cα' bonds must have a smaller dihedral angle with the most important spin con-

(14) (a) Howard, C. G.; Girolami, G. S.; Wilkinson, G.; Thornton-Pett, M.; Hursthouse, M. B. *J. Am. Chem. Soc.* **1984**, *106*, 2033.
(15) (a) Haaland, A. *Top. Curr. Chem.* **1975**, *53*, 1. (b) Almenningen, A.; Haaland, A.; Samdal, S. *J. Organomet. Chem.* **1978**, *149*, 219. (c) Freyberg, D. P.; Robbins, J. L.; Raymond, K. N.; Smart, J. C. *J. Am. Chem. Soc.* **1979**, *101*, 892. (d) *Fernholdt*, L.; Haaland, A.; Seip, R.; Robbins, J. L.; Smart, J. C. *J. Organomet. Chem.* **1980**, *194*, 351.
(16) Albright, T. A.; Burdett, J. K.; Whangbo, M.-H. *Orbital Interactions in Chemistry*; Wiley: New York, 1985; Chapter 20.
(17) Terpstra, A.; Louwen, J. N.; Oskam, A.; Teuben, J. H. *J. Organomet. Chem.* **1984**, *260*, 207.
(18) Schilling, B. E. R.; Hoffmann, R.; Lichtenberg, D. L. *J. Am. Chem. Soc.* **1979**, *101*, 585.
(19) Marynick, D. S. *J. Am. Chem. Soc.* **1984**, *106*, 4064.

Table III. Exchange Coupling Constants and Structural Data of Halogen-Bridged Manganese Complexes

compd	J, cm^{-1}	Mn–X,[a] Å	Mn–Mn*, Å	X–X,[a] Å	X–Mn–X, deg	Mn–X–Mn*, deg	ref
$[(Mecp)MnCl(PEt_3)]_2$ (2)	−4.8	2.482	3.515	3.503	89.8	90.2	
$[(Mecp)MnBr(PEt_3)]_2$ (3)	−5.0	2.631	3.672	3.768	91.5	88.5	
$[(Mecp)MnI(PEt_3)]_2$ (4)	−4.7	2.869[c]	3.927[c]	4.173[c]	93.5[c]	86.5[c]	
$Cs[MnCl_3]$[b] (14)	−9.8	2.551	3.181	3.455	85.2	77.1	22a, 23
$[Me_4N][MnCl_3]$ (15)	−4.4	2.560	3.25	3.429	84.1	78.7	22b, 23
$Cs[MnBr_3]$ (16)	−7.1	2.683	3.26	3.691	86.9	74.9	22c, 24
$Cs[MnI_3]$ (17)	−6.4	2.912	3.47	4.050	88.1	72.2	22d, 25

[a] Bridging halogen. [b] Structure different from 15–17; cf. text. [c] Mean value from two crystallographically independent molecules.

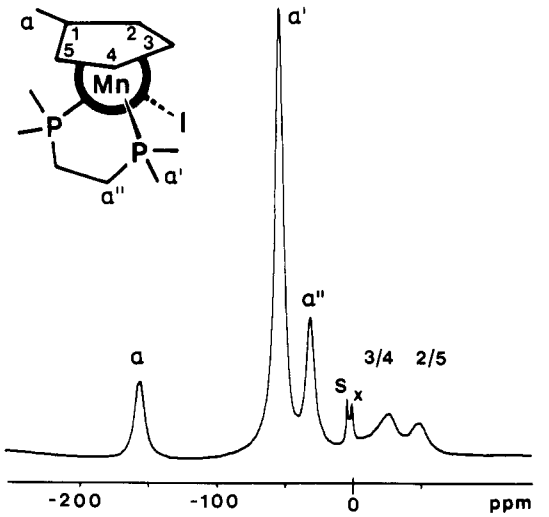

Figure 10. ^1H NMR spectrum of (Mecp)MnI(dmpe) (13) in CD_2Cl_2 at 303 K (S = solvent; X = impurity).

taining orbital than the P–Cα'' bond. Although the CpMX fragment orbitals interacting with those of dmpe are well-known from Hofmann's work,[20] a detailed qualitative analysis is too speculative because of the low symmetry of 13. The differences in spin density on Cα' and Cα'' are also reflected in the signal shifts of Hα' and Hα''. The fact that we observe only one Hα' signal is attributed to the above-mentioned dynamic behavior and/or very similar Hα' shifts. Work on diamagnetic low symmetry dmpe complexes shows that the expected number of signals may not be found in all cases.[21]

Since the molecular orbital diagram of manganese(II) half-sandwiches is similar to that of Cp_2Mn, the spin delocalization in high-spin manganocene (with π- and σ-delocalization as well as π-polarization being operative)[10] should also apply for the half-sandwiches. Actually, the ^1H NMR spectra of, e.g., $(Mecp)_2Mn$[10] and (Mecp)MnI$(PMe_3)_2$ (12) are rather similar (neglecting PMe_3) except that, at a given temperature, all Mecp signals of 12 appear at lower frequency than those of $(Mecp)_2Mn$ (with δ^{para} ($^1H2$–5) changing sign). This agrees nicely with our analysis of the spin delocalization[10] with a slight variation: in the half-sandwiches σ-delocalization is less efficient than in high-spin manganocenes while the combined π-pathways are similar.

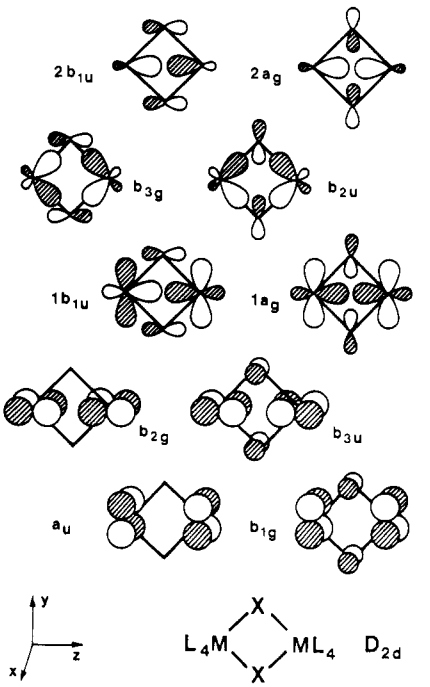

Figure 11. Frontier orbitals for $[CpMnXL]_2$.

Interaction in the Mn_2X_2 Four-Membered Ring. Both the structural data as well as magnetic exchange should provide insight in these interactions. As for transition-metal ions bridged by halides, very few series with a complete set of exchange coupling constants J and structural data for X = Cl, Br, and I are known. In Table III we compare our results with those of $M'MnX_3$. The latter series is not ideal because 15–17 contain linear chains with MX_6 octahedra sharing trigonal faces while 14 has similarly bridged trimers which share corners to give chains. Changing the gegenion as in 15 is known to influence J.[26]

First we draw attention to the decrease of the bridge angle Mn–X–Mn* on passing to the heavier halides. This is due to increasing repulsion of the halide p_y electrons (cf. Figure 11). The increasing radius of the halogen is reflected in Mn–X; actually, Mn–X of 2–4 is very close to the sum of the covalent radii. For simple geometric reasons, however, the X–X repulsion increases faster than Mn–X, and the molecule partly compensates for this effect by decreasing Mn–X–Mn*. For chlorine alone the halogen repulsion in dimers has been discussed by Ross and Stucky.[27]

No clear trend can be established for the change of J with the bridging halogen although an interesting corre-

(20) Hofmann, P.; Padmanabhan, M. *Organometallics* **1983**, *2*, 1273.
(21) (a) Bunker, M. J.; Green, M. L. H. *J. Chem. Soc., Dalton Trans.* **1981**, 85. (b) Kreiter, C. G.; Koemm, U. *Z. Naturforsch., B: Anorg. Chem., Org. Chem.* **1983**, *38B*, 943. (c) Pörschke, K. R.; Mynott, R.; Krüger, C.; Romão, M. J. *Z. Naturforsch., B: Anorg. Chem., Org. Chem.* **1984**, *39B*, 1076.
(22) Structural data partly calculated from references: (a) Li, T.-I; Stucky, G. D.; McPherson, G. L. *Acta Crystallogr., Sect. B: Struct. Crystallogr. Cryst. Chem.* **1973**, *29*, 1330. (b) Morosin, B.; Graebner, E. J. *Acta Crystallogr.* **1967**, *B23*, 766. (c) Goodyear, J.; Kennedy, D. J. *Acta Crystallogr., Sect. B: Struct. Crystallogr. Cryst. Chem.* **1972**, *B28*, 1640. (d) Seifert, H. J.; Krischka, K. H. *Thermochim. Acta* **1978**, *27*, 85.
(23) McCarthy, P. J.; Güdel, H. U. *Inorg. Chem.* **1984**, *23*, 880.
(24) Dingle, R.; Lines, M. E.; Holt, S. L. *Phys. Rev.* **1969**, *187*, 643.
(25) Zandbergen, H. W. *J. Solid State Chem.* **1980**, *35*, 367.
(26) Grey, I. E.; Smith, P. W. *Aust. J. Chem.* **1971**, *24*, 73.
(27) Ross, F. K.; Stucky, G. D. *J. Am. Chem. Soc.* **1970**, *92*, 4538.

lation of J with the angle M–X–M and/or the distance M–X has been worked out for bridged copper and chromium dimers by Hatfield and Hodgson.[28] For a better understanding of our results we present the four-membered ring orbitals relevant for magnetic exchange in Figure 11. Here we simplify the discussion by regarding $CpMn(PR_3)^+$ as a ML_4 fragment, the frontier orbitals[29] of which are all magnetic orbitals. When interaction between the orbitals of two ML_4 fragments and two halogens, arranged in D_{2h} symmetry, is allowed, the 10 orbitals in Figure 11 are obtained. Six of them have already been constructed by Kahn[30a] and Hoffmann.[30b] According to our results the energy spacing of the 10 orbitals in Figure 11 must be so small that all are singly occupied at ambient temperature.

The small effect of X on J reveals that the metal–metal interaction can be neglected as an exchange pathway. Even for the ML_4 $2a_1$ orbitals which are most susceptible to such an interaction[30b] and which are recognized in $2b_{1u}$ and $2a_g$, the Mn–Mn* distance is too long. There must be then sufficient overlap with the bridging halide orbitals so that the antiferromagnetic contribution dominates the exchange interaction. This can be expressed[31] by $J = -n^{-2}\sum^{n}_{i=1}|\Delta_i S_i|$, where J is half the energy separating the molecular triplet from the singlet state, n is the number of unpaired electrons in the monomer, Δ_i is the energy gap between the ith pair of bonding and antibonding orbitals in Figure 11, and S_i is the corresponding overlap integral.

From the equation it follows immediately that for such a high number of unpaired electrons $|J|$ should be small. It should be reduced further by Δ_i and S_i if the interaction in the M_2X_2 unit is weak. Such a situation is met obviously in **2–4** with rather long internuclear distances. A similar reasoning applies for **14–17** (cf. Table III). As for the small changes of J on going from **2** to **4**, we do not think that a detailed discussion is very conclusive at present. We note, however, that the halogen dependence of J in **2–4** parallels that in **15–17** and in $[Cp_2TiX]_2$.[32] The halogen dependence is actually a bridge angle dependence. It is therefore necessary to evaluate five Δ and S_i as a function of Mn–X–Mn* for the orbitals in Figure 11. Each Δ has a different angle dependence which in turn changes with the ligands of the ML_4 fragment; Δ may even pass through a minimum in the angle range of interest.[30b] Thus it is not surprising that we do not find a simple change of J with the bridging halogen.

Experimental Section

General Data. All organometallic compounds were handled under dry oxygen-free argon. Moisture and oxygen were removed from solvents by standard procedures. M. Barth, U. Graf, and G. Schuller from the microanalytical laboratory of this institute performed the elemental analyses.

Literature procedures were used to prepare the following compounds: PMe_3,[33] PEt_3,[33] 1,2-bis(dimethylphosphino)ethane (dmpe),[34] $AsEt_3$,[35] $MnCl_2$,[36] $MnBr_2$(1,2-dimethoxyethane),[37] MnI_2.[38] The synthesis of the starting manganocenes has been described in ref 10.

(η^5-Methylcyclopentadienyl)(μ-chloro)(tetrahydrofuran)manganese(II) Dimer (1). To a stirred mixture of 3.74 g (17 mmol) of 1,1′-dimethylmanganocene and 20 mL of THF was added 2.19 g (17 mmol) of $MnCl_2$. A slow color change from orange-red to light green accompanied by a slight increase in temperature was observed. After the solution was further stirred and boiled under reflux for 30 min, a clear solution was obtained. Concentration and successive addition of ether gave a crystalline material which was recrystallized from THF/ether to yield light green crystals of **1** (2.15 g, 51%). Anal. Calcd for $C_{20}H_{30}Cl_2Mn_2O_2$ (483.24): C, 49.71; H, 6.26; O, 6.62; Cl, 14.67; Mn, 22.74. Found: C, 49.19; H, 6.20; O, 6.97; Cl, 15.05; Mn, 23.33.

(η^5-Methylcyclopentadienyl)(μ-chloro)(triethylphosphine)manganese(II) Dimer (2). A solution of **1** in THF was prepared from 6.45 g (30 mmol) of 1,1′-dimethylmanganocene in ca. 20 mL of THF and 3.78 g (30 mmol) of $MnCl_2$. After addition of 15 g (127 mmol) of triethylphosphine at ambient temperature, the solution was kept under reflux for 1 h. Then most of the solvent was removed under vacuum, and ether was added until the solution became opaque. Storage at −25 °C gave a precipitate which was recrystallized from THF/pentane to give 13.5 g (78%) of light green crystals of **2**. Anal. Calcd for $C_{24}H_{44}Cl_2Mn_2P_2$ (575.34): C, 50.10; H, 7.71; Cl, 12.32; Mn, 19.10; P, 10.77. Found: C, 50.31; H, 7.75; Cl, 12.38; Mn, 18.49; P, 10.70.

(η^5-Methylcyclopentadienyl)(μ-bromo)(triethylphosphine)manganese(II) Dimer (3). A similar procedure as for **2** with 10.7 g (50 mmol) 1,1′-dimethylmanganocene, 14.8 g (49 mmol) of $MnBr_2$(1,2-dimethoxyethane), and 12 g (102 mmol) of triethylphosphine gave 25.5 g (77%) of dark green crystals of **3** from THF/ether. Anal. Calcd for $C_{24}H_{44}Br_2Mn_2P_2$ (664,24): C, 43.40; H, 6.68; Br, 24.06; Mn, 16.54; P, 9.33. Found: C, 43.36; H, 6.85; Br, 24.00; Mn, 15.81; P, 9.22.

(η^5-Methylcyclopentadienyl)(μ-iodo)(triethylphosphine)manganese(II) Dimer (4). Similar to **3**, 6.1 g (28 mmol) 1,1′-dimethylmanganocene, 8.74 g (28 mmol) MnI_2, and 7.7 g (65 mmol) triethylphosphine gave 12 g (57%) of green-blue needles. Anal. Calcd for $C_{24}H_{44}I_2Mn_2P_2$ (758.24): C, 38.02; H, 5.85; I, 33.47; Mn, 14.49; P, 8.17. Found: C, 37.78; H, 5.84; I, 33.58; Mn, 14.11; P, 8.27.

[η^5-(Trimethylsilyl)cyclopentadienyl](μ-iodo)(triethylphosphine)manganese(II) Dimer (5). Similar to **2**, 5.5 g (17 mmol) of 1,1′-(trimethylsilyl)manganocene, 5.2 g (17 mmol) of MnI_2, and 4 g (34 mmol) of triethylphosphine gave 9.4 g (63%) of green-blue needles of **5** after recrystallizing twice from ether. Anal. Calcd for $C_{28}H_{56}I_2Mn_2P_2Si_2$ (874.56): C, 38.46; H, 6.46; Mn, 12.56; P, 7.08. Found: C, 37.70; H, 6.25; Mn, 12.48; P, 7.00.

Bis(1,2-dimethoxyethane)manganese Diiodide. MnI_2 (7 g, 15 mmol) was placed in an argon-filled Soxhlet extractor, 250 mL of freshly dried and distilled 1,2-dimethoxyethane was added, and the extraction was run until almost all MnI_2 was transferred into the solvent flask. Then most of the solvent was removed in vacuo and the remainder cooled to −25 °C. Pink crystals (5.06 g, 68%) were obtained which are sensitive to oxygen, moisture, and light. IR (cm^{-1}): 2935 br, 2880 s, 2830 m, 1469 s, 1450 m, 1368 m, 1280 m, 1247 m, 1240 m, 1192 m, 1160 w, 1100 s, 1055 vs, 1025 m, 980 w, 867 m, 860 s, 832 m, 560 w, 395 w. Anal. Calcd for $C_8H_{20}I_2MnO_4$ (488.99): C, 19.65; H, 4.12; I, 51.90. Found: C, 19.03; H, 3.96; I, 51.39.

(η^5-1,2-Dimethylcyclopentadienyl)(μ-iodo)(triethylphosphine)manganese(II) Dimer (6). Similar to **3**, 0.5 g (2.1 mmol) of bis(1,2-dimethylcyclopentadienyl)manganese, 1.7 g (3.5 mmol) of bis(1,2-dimethoxyethane)manganese diiodide, and 0.6 g (8.6 mmol) of triethylphosphine gave 0.5 g (30%) of green smeary crystals of **6**.

Triethylarsine Adduct of Manganese Diiodide. To a slurry of 6.95 g (22.5 mmol) of MnI_2 in 100 mL of ether was added 7.3

(28) (a) Hatfield, W. E. In *Extended Interactions between Metal Ions*; Interrante, L. V., Ed.; ACS Symposium Series 5, American Chemical Society: Washington, DC, 1974; p 108. (b) Hodgson, D. J. *Ibid.* p 94.
(29) Elian, M.; Hoffmann, R. *Inorg. Chem.* **1975**, *14*, 1058.
(30) (a) Kahn, O.; Briat, B.; Galy, J. *J. Chem. Soc., Dalton Trans.* **1977**, 1453. (b) Saik, S.; Hoffmann, R.; Fisel, C. R.; Summerville, R. H. *J. Am. Chem. Soc.* **1980**, *102*, 4555.
(31) (a) Kahn, O.; Briat, B. *J. Chem. Soc., Faraday Trans. 2* **1976**, 1441. Cf. related equations in: (b) Hay, P. J.; Thibeault, J. C.; Hoffmann, R. *J. Am. Chem. Soc.* **1975**, *97*, 4884. (c) Leuenberger, B.; Güdel, H. U. *Inorg. Chem.* **1986**, *25*, 181.
(32) Coutts, R. S. P.; Martin, R. L.; Wailes, P. C. *Aust. J. Chem.*, **1973**, *26*, 2101.
(33) Wolfsberger, W.; Schmidbaur, H. *Synth. React. Inorg. Met.-Org. Chem.* **1974**, *4*, 149.
(34) Butler, S. A.; Chatt, J. *Inorg. Synth.* **1974**, *15*, 185.
(35) Friedrich, M. E. P.; Marvel, C. S. *J. Am. Chem. Soc.* **1930**, *52*, 378.
(36) Brauer, G. *Handbuch der präparativen anorganischen Chemie*; Enke: Stuttgart, 1981; Vol. III, p 1842.
(37) King, R. B. *Metal Organic Synthesis*; Academic Press: New York and London, 1965; Vol. I, pp 67–69.
(38) Biltz, W.; Hüttig, G. F. *Z. Anorg. Chem.* **1920**, *109*, 89.

g (45 mmol) of triethylarsine. While being stirred for 3 h at room temperature, the mixture turned orange-red. The solvent was removed in vacuo and the solid material recrystallized from ether/pentane at −20 °C to give pink crystals which analyzed for $[Mn_3I_6(AsEt_3)_4]_n$. The yield was 6.4 g (54% based on MnI_2). Anal. Calcd for $C_{24}H_{60}As_4I_6Mn_3$ (n = 1) (1574.64): C, 18.31; H, 3.84; I, 48.35. Found: C, 18.24; H, 3.76; I, 48.48.

(η^5-Methylcyclopentadienyl)(μ-iodo)(triethylarsine)manganese(II) Dimer (7). From 9.7 g (31.4 mmol) of MnI_2 in 100 mL ether and 10.18 g (62.8 mmol) of triethylarsine, the above arsine adduct was prepared. The reaction mixture was reacted directly with 6.75 g (31.4 mmol) of 1,1′-dimethylmanganocene leading to a deep green solution. About 60 mL of ether was removed in vacuo and 20 mL of pentane added. At −30 °C 23 g of deep green crystals formed. These were recrystallized from ether/pentane to yield 16.1 g (53%) of **7**. Anal. Calcd for $C_{24}H_{44}As_2I_2Mn_2$ (846.14): C, 34.06; H, 5.24; I, 30.00; Mn, 12.99. Found: C, 33.55; H, 5.05; I, 30.56; Mn, 13.44.

(η^5-Cyclopentadienyl)(μ-iodo)(triethylphosphine)manganese(II) Dimer (8). MnI_2 (7.66 g, 24.8 mmol) was suspended in 75 mL of THF. In an exothermic reaction the THF adduct[39] was formed. Without isolation, this was converted to $MnI_2(PEt_3)_2$[8] by addition of 5.85 g (49.6 mmol) of triethylphosphine under stirring. In the course of the latter reaction the precipitate of $MnI_2(THF)_2$ disappeared to give a dark solution which was heated to reflux for 10 min. When 12.4 mL of a 2.0 M solution of CpNa in THF was added, a dark green solution and a white precipitate was obtained. After the solution was boiled under reflux for 30 min, the solvent was evaporated and the residue extracted with 50 mL of toluene. About half of the toluene was replaced by pentane, and the solution was kept at −35 °C for 12 h to yield 3.91 g (43%; working up the mother liquor increases the yield) of dark green crystals of **8**. Anal. Calcd for $C_{22}H_{40}I_2Mn_2P_2$ (730.19): C, 36.19; H, 5.52; I, 34.76; Mn, 15.04; P, 8.48. Found: C, 36.21; H, 5.46; I, 34.49; Mn, 15.16; P, 8.77.

(η^5-Cyclopentadienyl)(μ-iodo)(trimethylphosphine)manganese(II) Dimer (9). Trimethylphosphine (4.53 g, 59.6 mmol) was added to a stirred suspension of 14.04 (45.5 mmol) of MnI_2 in 120 mL of ether. THF (ca. 20 mL) was also added so that the mixture was converted to a pink solution which most probably contained $MnI_2(PMe_3)_2$ by analogy to our earlier results.[8] Reaction with 15.3 mL of a 1.955 M solution of CpNa in THF gave a green solution and a white precipitate. The solvent was evaporated, the residue treated with 50 mL of toluene, and the extract brought to −40 °C. Dark green crystals (3.75 g, 32%) of **9** separated. From the mother liquor another 1.54 g of **9** was obtained, raising the yield to 44%. Elemental analyses were carried out from the first fraction. Anal. Calcd for $C_{16}H_{28}I_2Mn_2P_2$ (646.03): C, 29.75; H, 4.37; I, 39.29; Mn, 17.01. Found: C, 29.33; H, 4.15; I, 39.49; Mn, 17.26.

(η^5-Methylcyclopentadienyl)iodobis(trimethylphosphine)manganese(II) (12). In a suspension of 9.0 g (29.1 mmol) of MnI_2 in 100 mL of ether was poured 5.45 g (25.3 mmol) of 1,1′-dimethylmanganocene. Reaction took place under gentle warming, and the color changed to green. Since the MnI_2 contained a few percent of metallic manganese, 40 mL of THF were added to dissolve all the product. The manganese was separated, the solvents were evaporated, and the remainder was redissolved in a mixture of ca. 50 mL of ether and 2 mL of PMe_3. After prolonged cooling to −20 °C 7.9 g (38%; working up the mother liquor increases the yield) of light green crystals of **12** were obtained. Anal. Calcd for $C_{12}H_{25}IMnP_2$ (413.12): C, 34.89; H, 6.09; I, 30.72; P, 15.00. Found: C, 34.09; H, 5.93; I, 29.42; P, 14.33.

(η^5-Methylcyclopentadienyl)chlorobis(trimethylphosphine)manganese(II) (11). Similar to **12**, 2.12 g (16.8 mmol) of $MnCl_2$ in 50 mL of THF, 3.60 g (16.8 mmol) of 1,1′-dimethylmanganocene, and an excess of 7.3 g (96.0 mmol) of trimethylphosphine gave 9 g (83%) of light green crystals of **11**.

(η^5-Methylcyclopentadienyl)iodo[1,2-bis(dimethylphosphino)ethane]manganese(II) (13). The addition of 1.9 g (8.9 mmol) of 1,1′-dimethylmanganocene to a slurry of 2.8 g (9.1 mmol) of MnI_2 in 50 mL of ether gave a dark green solution with little solid material (presumably excess MnI_2 and metallic manganese still present from the synthesis of MnI_2). When 2.7 g (18.2 mmol) of 1,2-bis(dimethylphosphino)ethane was dropped into the stirred solution, the color vanished and an almost white precipitate formed. After removal of the ether the solid was extracted with about 50 mL of CH_2Cl_2, the solution was concentrated, and crystallization at −25 °C gave red-brown crystals which turned green at room temperature. The yield was 5.08 g (73%) of **13**. MS: m/z (relative intensity) 411 (0.03, M^+), 332 (0.3, (dmpe)MnI^+), 150 (4, dmpe$^+$), 134 (20, MecpMn$^+$), 79 (75, Mecp$^+$), 56 (38, Mn + 1^+) and intense peaks for [dmpe − nCH$_2$]$^+$. Anal. Calcd for $C_{12}H_{23}IMnP_2$ (411.10): C, 35.06; H, 5.64; I, 30.87; Mn, 13.36; P, 15.07. Found: C, 34.64; H, 5.50; I, 31.03; Mn 13.48; P, 14.89.

NMR Measurements. All spectra were run on a Bruker CXP 200 spectrometer equipped with a B VT 1000 temperature controller under conditions reported previously.[40] Solvent peaks served as internal references for the experimental paramagnetic shifts, δ_T^{expt}, at the measuring temperature T. These data were calculated relative to the shifts of the corresponding ligand nuclei of substituted ferrocenes[10] or the free donor ligands leading to the paramagnetic shifts, δ_T^{para}. Details are found in the supplementary material. Not all spectra could be recorded at the same temperature; on the other hand, it is desirable to compare the data of different compounds. We have therefore chosen 298 K as a standard temperature and calculated δ_{298}^{para} according to the Curie law if a temperature series was not available. We put up with the following systematic errors: (i) the NMR signal shifts of a ligand depend on whether it is free or bound in a diamagnetic complex. They also change depending on the type of complex. We are not aware of a complete appropriate data set of diamagnetic half sandwiches [(Rcp)MXL]$_2$ and (Rcp)MXL$_2$. Errors introduced by nonideal reference compounds are small for ^{1}H NMR data. (ii) The temperature-dependent studies show slight deviations from the Curie law. The accuracy of δ_T^{expt} was ±1 ppm for δ >100, or otherwise it was ±0.2 ppm; in the variable-temperature series it was ± 0.05 ppm for δ <6.

Magnetic Measurements. The Faraday method was used to determine the magnetic susceptibilities from 1.25 to 333 K. The measurements were performed with a 10-in. electromagnet (Bruker Physik) with Henry-type pole caps, a microbalance (Sartorius 4102), and a low-temperature device. Temperatures below 4.2 K were achieved by pumping off the helium reservoir with a Roots pump (Leybold-Heraeus WS-250) and connections having diameters ≥65 mm. Temperatures in the cryogenic range were measured with a gold/iron vs. chromel thermocouple and checked against the helium vapor pressure. A Pt and Ge resistor placed at the sample position was used to calibrate the thermocouple. The molar susceptibility, χ_m, was corrected for the diamagnetic contributions with 194, 204, and 220 × 10^{-6} cgs mol^{-1} for **2**, **3**, and **4**. χ_m^{corr} was converted to the effective magnetic moment via $\mu_{eff} = 2.828\ (\chi_m^{corr} T)^{1/2}$.

X-ray Structure Determinations. Single crystals of **2**, **3**, and **4** (from THF/pentane) were sealed under argon into glass capillaries and mounted directly on the diffractometer. The observed cell symmetries were checked by axial photographs and reduced cell calculations. The space groups were indicated unambiguously by the systematic absences. Exact cell constants were determined by least-squares refinement of the parameters of the orientation matrix to the setting angles of 15 high order reflections (**3**: 25 reflections) centered on the diffractometer. Crystal data and other numbers related to the structure determinations are summarized in Table IV. Data collection and refinement procedures followed closely those described in ref 41. Intensity data were corrected for Lp effects and those of **3** and **4** also for absorption. For the latter an empirical correction based on scans at intervals of 10 deg around the diffraction vectors of nine selected reflections (**4**: seven reflections) near χ = 90° was used.

The structure of **2** was solved by Patterson methods. A series of full-matrix least-squares refinements, followed by difference Fourier syntheses, gave all non-hydrogen atoms. Since **3** is iso-

(39) Hosseiny, A.; McAuliffe, C. A.; Minten, K.; Parott, R.; Pritchard, R.; Tames, J. *Inorg. Chim. Acta* **1980**, *39*, 227.

(40) (a) Köhler, F. H.; Hofmann, P.; Prössdorf, W. *J. Am. Chem. Soc.* **1981**, *103*, 6359. (b) Köhler, F. H.; Geike, W. *J. Magn. Reson.* **1983**, *53*, 297.

(41) Karsch, H. H.; Appelt, A.; Müller, G. *Organometallics* **1985**, *4*, 1624.

Table IV. Crystal Structure Data of 2, 3, and 4

	2	3	4
formula	$C_{24}H_{44}Cl_2Mn_2P_2$	$C_{24}H_{44}Br_2Mn_2P_2$	$C_{24}H_{44}I_2Mn_2P_2$
M_r	575.34	664.24	758.25
cryst system	orthorhombic	orthorhombic	monoclinic
space group	*Pbca*	*Pbca*	$P2_1/c$
a, Å	13.691 (3)	13.869 (1)	15.099 (4)
b, Å	15.314 (2)	15.248 (1)	15.365 (3)
c, Å	14.402 (3)	14.540 (1)	14.576 (4)
α, deg	90	90	90
β, deg	90	90	108.11 (2)
γ, deg	90	90	90
V, Å^3	3019.6	3074.8	3214.1
d_{calcd}, g cm^{-3}	1.265	1.435	1.567
Z	4	4	4
μ, cm^{-1}	11.0	34.8	27.7
$F(000)$, e	1208	1352	1496
T, °C	22	22	22
radiation	Mo Kα	Mo Kα	Mo Kα
λ, Å	0.710 69	0.710 69	0.710 69
diffractometer	Syntex $P2_1$	CAD4	Syntex $P2_1$
hkl range	+14,+16,+15	+17,+19,+18	+15,+16,±16
$((\sin\theta)/\lambda)_{max}$, Å^{-1}	0.572	0.648	0.606
scan	ω	ω–2θ	ω
$\Delta\omega$, Å	0.9	0.8 + 0.35 tan θ	0.9
refl unique	1976	3479	5061
refl obsd	1611[a]	1572[b]	2697[b]
param refined	156	136	227
R[c]	0.055	0.046	0.071
R_w[d]	0.055	0.033	0.081
$\Delta\rho$(max/min), e/Å^3	+0.39/−0.29	+0.45/−0.46	+0.71/−0.86

[a] $F_o \geq 2.0\sigma(F_o)$. [b] $F_o \geq 4.0\sigma(F_o)$. [c] $R = \sum(||F_o| - |F_c||)/\sum|F_o|$. [d] $R_w = [\sum w(|F_o| - |F_c|)^2/\sum wF_o^2]^{1/2}$.

Table V. Fractional Atomic Coordinates and Equivalent Isotropic Temperature Factors of 2[a]

atom	x	y	z	U_{eq}, Å^2
Mn	0.43695 (8)	−0.09710 (7)	0.52520 (8)	0.049
Cl	0.41473 (14)	0.02443 (13)	0.41311 (13)	0.060
P	0.31334 (13)	−0.04877 (12)	0.64897 (13)	0.047
C1	0.4806 (9)	−0.2542 (6)	0.5576 (7)	0.087
C2	0.3743 (9)	−0.2547 (6)	0.5466 (9)	0.091
C3	0.3514 (10)	−0.2257 (7)	0.4562 (10)	0.105
C4	0.4383 (12)	−0.2103 (6)	0.4081 (8)	0.109
C5	0.5171 (8)	−0.2267 (5)	0.4697 (8)	0.085
C1′	0.5391 (11)	−0.2802 (8)	0.6417 (9)	0.149
C10	0.1846 (6)	−0.0733 (6)	0.6229 (6)	0.071
C11	0.1493 (6)	−0.0321 (7)	0.5321 (7)	0.092
C12	0.3167 (6)	0.0692 (5)	0.6674 (5)	0.056
C13	0.2473 (7)	0.1069 (6)	0.7400 (6)	0.082
C14	0.3290 (6)	−0.0968 (5)	0.7653 (5)	0.060
C15	0.4269 (6)	−0.0740 (6)	0.8092 (5)	0.075

[a] ($U_{eq} = (U_1U_2U_3)^{1/3}$, where U_i are the eigenvalues of the $\mathbf{U}_{ij}$ matrix).

Table VI. Fractional Atomic Coordinates and Equivalent Isotropic Temperature Factors of 3

atom	x	y	z	U_{eq}, Å^2
Br	0.4091 (1)	0.0302 (1)	0.4091 (1)	0.052
Mn	0.4323 (1)	−0.1006 (1)	0.5254 (1)	0.043
P	0.3150 (1)	−0.0483 (1)	0.6499 (1)	0.042
C1	0.4689 (8)	−0.2574 (6)	0.5525 (6)	0.063
C2	0.3689 (9)	−0.2557 (6)	0.5466 (8)	0.072
C3	0.3450 (6)	−0.2281 (6)	0.4612 (10)	0.094
C4	0.4284 (11)	−0.2129 (6)	0.4136 (6)	0.084
C5	0.5056 (6)	−0.2326 (6)	0.4689 (8)	0.063
C1′	0.5233 (9)	−0.2863 (6)	0.6333 (8)	0.128
C10	0.1877 (5)	−0.0702 (5)	0.6279 (5)	0.060
C11	0.1519 (5)	−0.0308 (6)	0.5372 (5)	0.081
C12	0.3214 (5)	0.0703 (4)	0.6657 (5)	0.048
C13	0.2590 (6)	0.1104 (5)	0.7412 (5)	0.066
C14	0.3297 (4)	−0.0964 (4)	0.7642 (4)	0.049
C15	0.4260 (5)	−0.0759 (4)	0.8083 (4)	0.062

structural with **2**, the heavy-atom positions (Cl, Mn, P) of **2** served as starting point of the refinement. **4** was solved by direct methods (SHELX76). **2** and **3** were refined with anisotropic thermal parameters. Thereby the ethyl carbon atoms of **2** were treated as rigid groups including their H atoms, while all other H atoms were neglected. For **3** 11 H-atom positions out of a total of 22 were taken from difference Fourier syntheses. The remainder was calculated at idealized geometrical positions (XANADU). Thereby found H atoms served to determine the conformations

Table VII. Fractional Atomic Coordinates and Equivalent Isotropic Temperature Factors of 4

atom	x	y	z	U_{eq}, Å^2
I1	0.5408 (1)	0.4247 (1)	0.4021 (1)	0.069
I2	1.0761 (1)	0.5677 (1)	0.1246 (1)	0.070
Mn1	0.3945 (2)	0.4202 (2)	0.4886 (2)	0.060
Mn2	0.8959 (2)	0.4876 (2)	0.0516 (2)	0.061
P1	0.4721 (5)	0.3127 (4)	0.6262 (5)	0.074
P2	0.9392 (5)	0.3445 (4)	0.1464 (5)	0.077
C1	0.2228 (17)	0.4412 (23)	0.4693 (22)	0.081
C2	0.2375 (17)	0.3484 (17)	0.4683 (23)	0.079
C3	0.2672 (20)	0.3200 (21)	0.3909 (26)	0.100
C4	0.2718 (23)	0.3970 (33)	0.3390 (22)	0.113
C5	0.2473 (20)	0.4731 (21)	0.3884 (27)	0.085
C6	0.1852 (21)	0.4957 (23)	0.5373 (27)	0.124
C101	0.7216 (17)	0.5128 (20)	−0.0120 (30)	0.073
C102	0.7346 (21)	0.4914 (23)	0.0855 (24)	0.090
C103	0.7973 (17)	0.5626 (23)	0.1354 (22)	0.081
C104	0.8140 (24)	0.6186 (20)	0.0653 (38)	0.101
C105	0.7728 (22)	0.5887 (22)	−0.0268 (22)	0.096
C106	0.6695 (22)	0.4777 (26)	−0.1017 (29)	0.146
C10	0.4604 (21)	0.1916 (20)	0.5976 (22)	0.120
C11	0.4964 (24)	0.1731 (22)	0.5166 (24)	0.134
C12	0.5990 (18)	0.3307 (17)	0.6768 (18)	0.092
C13	0.6542 (21)	0.2650 (20)	0.7618 (22)	0.120
C110	1.0317 (27)	0.2846 (26)	0.1161 (27)	0.158
C111	1.0588 (32)	0.1929 (31)	0.1531 (32)	0.199
C112	0.8476 (22)	0.2636 (20)	0.1278 (23)	0.122
C113	0.8013 (23)	0.2457 (22)	0.0237 (24)	0.131
C14	0.4491 (31)	0.3329 (29)	0.7431 (31)	0.075
C15	0.3577 (37)	0.3465 (34)	0.7323 (36)	0.095
C114	1.0127 (39)	0.3484 (35)	0.2774 (37)	0.102
C115	0.9452 (62)	0.3752 (57)	0.3198 (60)	0.190
C16	0.4061 (44)	0.2987 (43)	0.7200 (44)	0.128
C17	0.4115 (42)	0.3946 (40)	0.7657 (42)	0.118
C116	0.9265 (66)	0.3413 (64)	0.2684 (68)	0.206
C117	0.9709 (51)	0.4170 (51)	0.3319 (52)	0.156

of all methyl groups. They were included as fixed-atom contributions in the refinement. Refinement of **4** was severely hampered by excessive disorder of the ethyl groups. Final refinement was done with isotropic thermal parameters for the ethyl carbons and one ethyl group of each independent molecule in two different conformations. H atoms were not included in the refinement. A final difference synthesis still gave indications for further partially occupied ethyl group alternatives.

The function minimized was $\sum w(|F_o| - |F_c|)^2$, with unit weights for **2** and **4**, while statistical weights were used for **3** (SHELX76). Corrections for $\Delta f'$ and $\Delta f''$ were applied to all atoms. Reference 41 gives the sources of the scattering curves as well as references to the programs used. Table II contains important bond distances and angles; Tables V–VII contain the atomic parameters. Figure 7 gives perspective views of **3** and **4**.

Other Physical Measurements. The IR data were obtained from KBr disks with a Perkin-Elmer 577 spectrometer and the MS data from a Varian MAT 311A spectrometer (EI, 70 eV). The molecular weights were determined cryoscopically in benzene with a homemade glassware apparatus equipped for inert-gas manipulation. The temperature was determined with a Knaur low-temperature measuring device with type F 22 sensor. We thank M. Barth for these measurements.

Acknowledgment. We gratefully acknowledge support by the Fonds der Chemischen Industrie, Frankfurt, and the BASF AG, Ludwigshafen.

Registry No. **1**, 92421-50-6; **2**, 92421-53-9; **3**, 92421-54-0; **4**, 92421-55-1; **5**, 105335-44-2; **6**, 105335-45-3; **7**, 105335-46-4; **8**, 105335-47-5; **9**, 105335-48-6; **10**, 105335-49-7; **11**, 105335-50-0; **12**, 92421-56-2; 1,1′-dimethylmanganocene, 32985-17-4; 1,1′-(trimethylsilyl)manganocene, 101932-73-4; bis(1,2-dimethoxyethane)manganese diiodide, 105335-52-2; bis(1,2-dimethylcyclopentadienyl)manganese, 101932-74-5.

Supplementary Material Available: Tables of experimental NMR shifts including variable-temperature data, variable-temperature magnetic susceptibilities, and magnetic moments at different field strengths, crystal data, fractional coordinates, and anisotropic temperature factors (26 pages); listings of observed and calculated structure factor amplitudes (22 pages). Ordering information is given on any current masthead page.

Activation Volumes for the Substitution Reactions of the Triruthenium Cluster Anions $HRu_3(CO)_{11}^-$ and $Ru_3(CO)_{11}(CO_2CH_3)^-$

Douglas J. Taube,[1] Rudi van Eldik,*[2] and Peter C. Ford*[1]

Institute for Physical Chemistry, University of Frankfurt, 6000 Frankfurt/Main, FGR, and Department of Chemistry, University of California, Santa Barbara, California 93106

Received May 28, 1986

Pressure effects on the stopped-flow kinetics for the reaction $HRu_3(CO)_{11}^- + PPh_3 \rightarrow HRu_3(CO)_{10}(PPh_3)^- + CO$ in tetrahydrofuran have been used to calculate the activation volume $\Delta V^\ddagger = +21.2 \pm 1.4$ cm^3/mol. This result is interpreted as confirming the dissociative mechanism previously proposed for this reaction. Analogous studies on the reaction of $P(OCH_3)_3$ with the methoxycarbonyl adduct $Ru_3(CO)_{11}(CO_2CH_3)^-$ in 90/10 THF/CH_3OH gives a similarly large positive $\Delta V^\ddagger$ (+16 ± 2 cm^3/mol) also consistent with a previously proposed dissociative mechanism for this reaction. However in the more protic solvent mixture 10/90 THF/CH_3OH, $\Delta V^\ddagger$ for the latter reaction is nearly zero, a result which suggests a markedly greater role of solvation changes in the rate-limiting step in this medium.

Introduction

The trinuclear ruthenium hydride ion $HRu_3(CO)_{11}^-$ has drawn considerable recent attention as a prominent species in homogeneous catalysts for the water-gas shift reaction[3] and for the hydrogenation, hydroformylation, and hydrosilation of alkenes.[4] In the course of investigating the reactivity of $HRu_3(CO)_{11}^-$ and its potential roles in such catalytic cycles, this ion was found to be remarkably more labile toward ligand substitution (eq 1) than the parent neutral carbonyl $Ru_3(CO)_{12}$ under comparable conditions.[5]

$$HRu_3(CO)_{11}^- + PPh_3 \rightleftharpoons HRu_3(CO)_{10}(PPh_3)^- + CO \quad (1)$$

A similarly enhanced substitution lability (eq 2) has also been described[6] for the methoxide adduct $Ru_3(CO)_{11}(CO_2CH_3)^-$, which is a likely intermediate in reactions such as the $Ru_3(CO)_{12}/NaOCH_3$ cocatalyzed reductive carbonylation of nitroarenes.[7] Previous kinetics studies have concluded that both reactions 1 and 2 are likely to proceed via dissociative mechanisms[5,6] and that it is this dissociative process which makes the latter anion particularly reactive toward dihydrogen (eq 3).[6] However, not only

$$Ru_3(CO)_{11}(CO_2CH_3)^- + P(OCH_3)_3 \rightarrow Ru_3(CO)_{10}(CO_2CH_3)(P(OCH_3)_3)^- + CO \quad (2)$$

$$Ru_3(CO)_{11}(CO_2CH_3)^- + H_2 \rightarrow HRu_3(CO)_{11}^- + HCO_2CH_3 \quad (3)$$

(1) University of California.
(2) University of Frankfurt.
(3) (a) Ford, P. C. *Accounts Chem. Res.* **1981**, *14*, 31–37. (b) Gross, D. C.; Ford, P. C. *J. Am. Chem. Soc.* **1985**, *107*, 585–593. (c) Bricker, J. C.; Nagel, C. C.; Shore, S. G. *J. Am. Chem. Soc.* **1982**, *104*, 1444–1445. (d) Bricker, J. C.; Nagel, C. C.; Bhattacharyya, A. A.; Shore, S. G. *J. Am. Chem. Soc.* **1985**, *107*, 377–384.
(4) (a) Süss-Fink, G. *Angew. Chem., Int. Ed. Engl.* **1982**, *21*, 73–74. (b) Süss-Fink, G.; Ott, J.; Schmidkonz, B.; Guldner, K. *Chem. Ber.* **1982**, *115*, 2487–2493. (c) Süss-Fink, G.; Reiner, J. *J. Mol. Catal.* **1982**, *16*, 231–242.
(5) Taube, D. J.; Ford, P. C. *Organometallics*, **1986**, *5*, 99–104.
(6) (a) Anstock, M.; Taube, D.; Gross, D. C.; Ford, P. C. *J. Am. Chem. Soc.* **1984**, *106*, 3696–3697. (b) Taube, D. J.; Rokicki, A.; Anstock, M.; Ford, P. C., submitted for publication.
(7) Alper, H.; Hashem, K. E. *J. Am. Chem. Soc.* **1981** *103*, 6514–6515.

0276-7333/87/2306-0125$01.50/0